Free-Flight Investigation of High-Maneuverability Missile Dynamics

Martin E. Beyers*
South African Council for Scientific and Industrial Research, Pretoria, South Africa

The practicability of wind-tunnel free-flight testing of high-maneuverability vehicles has been realized by the introduction of new concepts for model launching and trajectory design, and a technique for analysis of nonoscillatory motion at angles of attack. A canard missile is investigated at Mach 0.7 for center-of-mass positions ranging from stable to bistable (statically unstable at low angles) and angles of attack up to 25°. The effect of oscillation frequency on dynamic stability is explored. Static stability coefficients obtained from angular motion peaks are presented here for the first time. A computer simulation based on the free-flight results, which indicated satisfactory agreement with observed motion, and a correlation of free-flight and sting test data, revealed a possible inadequacy of the latter.

Nomenclature

C_{L_α}	= lift curve slope (rad $^{-1}$)
$C_{L_q}+C_{L_{\dot\alpha}}$	= lift due to pitching and plunging
C_m	= pitching moment coefficient
C_{m_α}	= pitching-moment curve slope (rad $^{-1}$)
$C_{m_q}+C_{m_{\dot\alpha}}$	= effective pitch-damping coefficient
d	= reference length
E	= relative angular excursion
I_y, I_x	= moments of inertia in pitch and roll
m	= mass
p	= roll rate (deg/m)
t	= time
X, Y, Z	= inertial reference system
x_{cg}	= center of mass aft of nose
X_T, Y_T, Z_T	= tunnel coordinate system
α, β	= angles of attack and sideslip
$\alpha_{min}, \alpha_{max}$	= minimum and maximum angles
α_{trim}	= trim angle of attack
$\bar\alpha$	= local angle of attack
$\bar\alpha_R$	= resultant angle of attack
δ^2	= mean-square resultant angle of attack
ξ	= complex angle of attack
ψ, θ, ϕ	= Euler angles
θ_z	= vertical-plane projection of θ
$\omega d/V$	= reduced frequency

Subscripts

0	= with coefficients, $\alpha = 0$; otherwise $t = 0$
1	= linear analysis
3	= local analysis
EFF	= effective
m	= mean

Introduction

THE comparatively recent trend toward increased maneuverability and/or higher angles of attack in missile design has compounded difficulties involved in the dynamic stability predictions. This is particularly true in the case of canard-controlled missiles, where wing-tail interference effects give rise to pronounced nonlinearities in the aerodynamic coefficients, even at low angles of attack. In the absence of any reliable analytical method it has been necessary to rely almost completely on experimental and empirical techniques.

The validity of missile motion simulations based on wind tunnel data are clearly qualified by the assumption that static sting test data, and dynamic stability data extracted as effects present in constrained motion on a support, are representative of behavior in flight. While there may be a basis for such an assumption, in many cases, it becomes suspect when applied to highly maneuverable flight vehicles which are characterized by nonlinear responses with concomitant pitching, plunging, and coning motions. In these circumstances, it is eminently desirable to test models under conditions of motion in six degrees of freedom. While this could, in prinicple, be achieved in a ballistic range, such tests have been avoided to date due to the large lateral displacements exhibited by destabilized models, in favor of tests using models with forward centers of mass.[1]

Dynamic stability data have been obtained in wind tunnels on configurations such as re-entry bodies[2] and finned missiles[3] by studying the flight of oscillating models. However, in all dynamic-stability free-flight tests on reasonably large model scales only stable, oscillating models appear to have been considered.

The main objective of this paper is to present techniques for wind-tunnel free-flight testing of high-maneuverability configurations in nonoscillatory motion at angles of attack and to demonstrate their effectiveness in evaluating a destabilized, canard missile test configuration at Mach 0.7.

New trajectory design concepts, introduced here, and a pitch-jet model launching system, described in detail elsewhere,[4] have made possible full utilization of available observation space in a conventional wind tunnel. Data reduction is accomplished by a procedure developed for roll-rate determination, and techniques for data smoothing[5] and local aerodynamic analysis.[6]

Methods of Approach

The free-flight models tested are depicted in Fig. 1. Marginal static-stability configurations were obtained using aft center-of-mass locations to be representative of a class of cruciform, canard missiles which have a bistable (stable-unstable-stable) pitching moment characteristic. Since low roll rates and moderate or low angles of attack are pertinent design criteria, and by virtue of the low natural frequencies, they are susceptible to resonance instability and roll-trim interaction. The associated large lateral displacements and high damping rates, which make it difficult to sustain any oscillatory motion, complicate the free-flight test situation.

Presented at the AIAA 9th Aerodynamic Testing Conference, Arlington, Texas, June 7-9, 1976 (in bound volume of Conference papers, no paper number); submitted July 19, 1976; revision received Nov. 10, 1976.

Index categories: LV/M Dynamics, Uncontrolled; LV/M Simulation.

*Chief Research Engineer, Aeronautics Research Unit. Member AIAA.

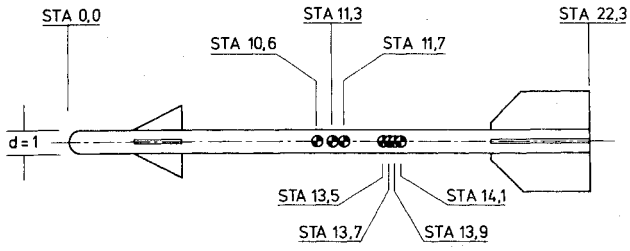

Fig. 1 Test configurations.

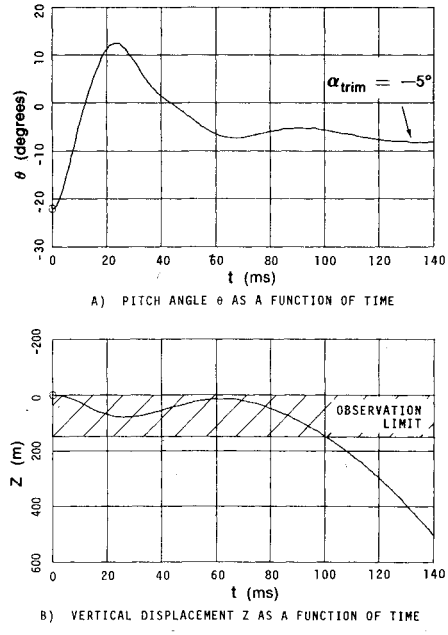

Fig. 2 Simulated flight of a bistable model.

Concepts for Trajectory Design

Usually models were designed simply to maximize the observable number of cycles and the amplitude decay.[7] In the present case, many additional parameters, including launch-gun release point, launch angle, initial angle of attack and launch velocity, have to be taken into account along with model physical parameters in order to optimize each particular test situation.

To illustrate this point a simulation was made of a typical flight of the missile model as shown in Fig. 2. The motion is highly damped and quickly settles down to a trim angle of attack of $-5°$ due to its bistable pitching moment. A closer inspection reveals a slight "kink" in the top curve near 40 ms. If the initial amplitude θ_0 should be reduced from 22° to 20°, and flow parameters remain unchanged, the curve will turn upwards at this point (due to insufficient angular momentum) and fall into a positive trim angle $+5°$. There is thus a minimum value of θ_0 corresponding to the number of complete cycles required, accompanied by a minimum vertical swerve displacement.

Swerve can be reduced by resorting to a smaller ratio I_y/md^2. Should the mass be unchanged and I_y reduced, the frequency will increase and the trim condition be reached in a shorter time, making it more difficult to observe the initial oscillation peaks. Hence a larger mass is indicated. On the other hand, it may be more expedient to use a smaller mass in order that higher launch velocities may be used to expand the flight portion before the trim point, after which the vertical displacement rapidly grows beyond the limits of observation. Further, a value of the ratio I_y/md^2 can be found which will maximize the distance S travelled relative to the observation window during one oscillation cycle, a realistic criterion when only one cycle can be observed. In the simple case of an oscillating model with constant drag coefficient and linear aerodynamics, a maximum distance per cycle is obtained when

$$m = \frac{\pi^2}{2}\,\frac{I_y}{dS}\,\frac{C_D}{-C_{m_\alpha}}$$

These contradictory requirements for the mass parameters are further complicated by practical problems associated with the fabrication of high-fineness-ratio models. Hence it can be very difficult to arrive at a truly optimal design.

It is shown here that the test situation can be improved considerably by optimal choice of initial conditions at launching. Details of the launch gun and associated equipment have been presented elsewhere.[8] The simplest method of launching a model at incidence, as applied to stable models, is to support it at the desired angle during acceleration. In contrast, bistable models are launched at zero angle relative to the launch gun and imparted an angular acceleration which causes the maximum angle of attack to be developed only after the model comes into the field of view. This means that larger angles and higher frequencies can be achieved so that an additional oscillation cycle or portion of a cycle may be observed. The principle is realized by the "pitch-jet" launch head. At the end of its acceleration stroke the launcher piston is decelerated and the model travels forward, guided between a rail and a shroud. A double air-jet, fed by compressed air within the launch-gun piston, blows on the model tail after it is free of the rail to initiate a nose-up pitching motion.

A concomitant of the jet thrust is a downward velocity component which, when combined with an additional component due to a suitable launch-gun depression angle θ_G, can compensate effectively for the initial tendency to swerve upwards. Taking the concept a step further, the model can be allowed to travel downwards by using an appropriately larger depression θ_G. This position of the launch gun is shown by the solid lines in Fig. 3, which illustrates the different launch configurations. With an initial downwards displacement, the model becomes free of interference sooner as its wake quickly

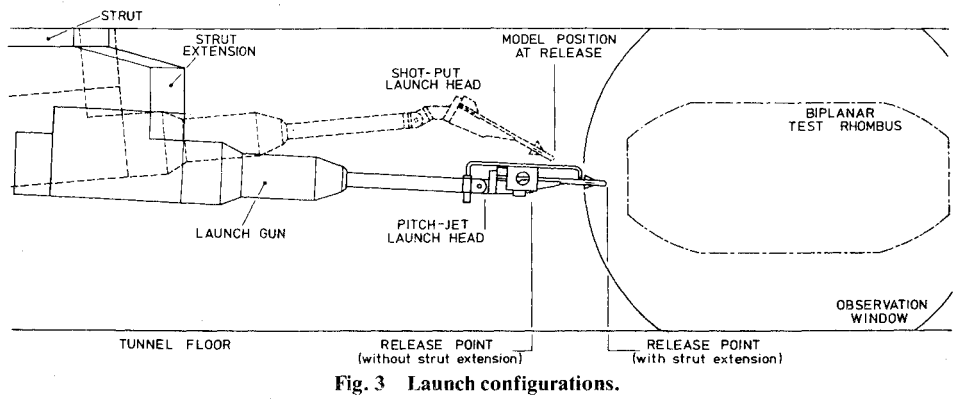

Fig. 3 Launch configurations.

passes below the launch head. As a result the release point may be located adjacent to the downstream side of the biplanar observation rhombus[8] using an extension to the support strut as shown in Fig. 3.

Initial conditions for a model launched in this way are determined from the equations of motion for launch-gun/model separation: The angular motion equations are of the form

$$\dot{\theta}^2 = A_2\theta^2 + A_1\theta + A_0 + \dot{\theta}_0^2$$

$$\theta = \{D_1 \sinh(A_2^{1/2}t + D_0) - A_1\}/2A_2 \qquad (1)$$

where θ is the model inclination to the launch gun axis and A_0, A_1, A_2, D_0 and D_1 are constants. The technique was found to be convenient to use and capable of producing repeatable results, and is discussed in detail in another paper.[4]

Free-flight models used in these tests have to satisfy stringent requirements for symmetry. Small misalignments between canard and tail surfaces, for example, produce unpredictable flight behavior which may mean that the model is prematurely lost from view. To overcome this problem, models were assembled using machined metal and/or injection-molded polystyrene components accurately located by telescopic-tubing body sections. The model length was 161.4 mm, corresponding to a body diameter of 7.25 mm.

Model design criteria discussed above imply a different ratio I_y/md^2 (and sometimes mass) for each center-of-mass configuration tested. A computer program[8] was used to facilitate the design of models used in these studies. Models with identical mass and centers of mass but different moments of inertia ($I_y = 360$ g-cm^2 and 1100 g-cm^2), were used to investigate frequency effects on dynamic stability.

Data Reduction Procedure

The limited number of angular excursions, large amplitude decay and nonconstant roll rates typical of the destabilized configuration, pose particular problems for data reduction.

Requirements for Data Acquisition

Since nonlinear aerodynamic effects on observed free-flight motion can be determined only when they are not masked by data scatter nor distorted by calibration errors, the emphasis here is on accuracy. The starting point is clearly to obtain a precise alignment of the optical system.

Model flights are recorded by high-speed photography through a nonorthogonal biplanar optical system.[8] The problem of determining the orientation of the individual front-surfaced plane mirrors relative to each other and to the tunnel reference system, was solved by the introduction of a "reflecting theodolite." This device, comprising a conventional theodolite in which the objective lens is replaced by a high-quality plane mirror, made it possible to measure light beam directions to within ± 10 sec. A survey of the biplanar field showed that the variation in light-path direction along the tunnel-centerline vertical plane was less than ± 15 sec. In the worst case, this introduces a minuscule error of 0.004° in the measured angles.

The film analysis procedure consists of determining model position X_1, ζ_1 and X_2, ζ_2 and orientation θ_1, θ_2 relative to a reference grid, on each half-frame, using a template/image matching system, and determining roll angles ϕ by measuring the apparent wingspan on successive frames. The biplanar transformation equations are

$$Y_T = (\zeta_2 \cos\sigma_1 - \zeta_1 \cos\sigma_2)/\sin(\sigma_2 - \sigma_1) \qquad (2a)$$

$$Z_T = (\zeta_2 \sin\sigma_1 - \zeta_1 \sin\sigma_2)/\sin(\sigma_1 - \sigma_2) \qquad (2b)$$

where σ_2 and σ_1 are the top and bottom viewing angles respectively. Equations for the biplanar angle transformation are obtained simply by division of Eq. (2) by a length equal to the horizontal projection of the model on the reference grid. The equation for roll reduction, applicable to near-planar motion, is

$$\phi = N\frac{\pi}{2} + \{1 + (-1)^j\}\frac{\pi}{4} + (-1)^{j-1}\cos\frac{s_a}{s} \quad j = 1,2\ldots \qquad (3)$$

where N is the number of quarter cycles completed and s_a and s are the apparent and actual wingspans respectively. Roll directions could be observed by means of front-lighting. The exact transformation of nonplanar roll data, not given here, was obtained after determining the roll angle in an inclined coordinate system.

Analysis of Angular Data

A model-dependent data reduction procedure may yield erroneous results when applied to very short flights. The Chapman-Kirk technique,[9] though well-suited when there are several oscillation cycles, may not converge on a correct solution when less than one cycle is present.

Angular data are analyzed here by applying a smoothing procedure[5] in conjunction with a local curve-fitting technique.[6] A smoothed data set is found by superposition of a primary tricyclic solution

$$\xi_1 = K_1 e^{i\phi_1} + K_2 e^{i\phi_2} + K_3 e^{i\phi_3} \qquad (4)$$

and a series of small-amplitude tricycles obtained by curve-fitting the residuals, so that

$$\xi = \beta + i\alpha = \sum_{j=1}^{n} (\beta_{cj} + i\alpha_{cj}) \qquad (5)$$

where each component has the form of the tricyclic equation. The smoothing is therefore accomplished by a process through which the linear solution, Eq. (4), is complimented by a number of free constants to account for the nonlinearities. While physical interpretation of the additional motion constants is hampered by the presence of nonaerodynamic fluctuations, validity of the technique is demonstrated by its capability of reconstructing angular motion from experimental data with random errors: In the case of exact data generated for the missile model, with superimposed random errors of 0.5% to 5% of α_{max}, the reconstructed motions matched the original motion very closely.

Aerodynamic analysis of the smoothed motion proceeds quite independently of the smoothing function. By fitting Eq. (4) to very short flight segments (ca 1/8 wavelength) at the angular peaks, the aerodynamic coefficients extracted have essentially local values as the angle of attack, roll rate, and velocity do not deviate appreciably from the mean values. Local C_{m_α} data are correlated with the local angle of attack $\bar{\alpha}$ for intervals with the same relative angular excursion

$$E = (\alpha_{max} - \alpha_{min})/\bar{\alpha} \qquad (6)$$

The dynamic stability coefficient, $C_{mq} + C_{m_{\dot{\alpha}}}$, is determined from linear curve fits of one- to two-wavelength segments of the smoothed data. However, the Chapman-Kirk technique would be more appropriate where two or more cycles have been observed.

Analysis of Swerve Data

Lateral displacements of the missile in flight are large, particularly in the case of nonoscillating flight where the angle contributions due to swerve may be of the order of 2°. Swerve corrections

$$\alpha = \theta_z + \tan^{-1}\frac{dz}{dx} \qquad \beta = -\psi + \tan^{-1}\frac{dy}{dx} \qquad (7)$$

are determined from a linear curve fit of Nicolaides' lift equation[10] to the displacement data. Since this equation is evaluated by first integrating the tricyclic equation, the linear solution must satisfy requirements for an accurate fit of the swerve data, after which the primary fit in the smoothing process can be determined. For variable roll rates, the validity of this curve fit is dependent on a suitable value of p (see below).

When the deviation between experimental and computed swerve data becomes too large, the transformation to aeroballistic coordinates is invalid. Consequently, a portion of the flight must be considered, or alternatively a nonlinearity introduced in the lift equation. The criterion used in the present analysis is that angle corrections determined for a complete flight should not deviate by more than 0.04° from those computed from a fit of the first oscillation cycle, where a very low rms error can usually be attained.

Nonconstant Roll Rate

Roll rates were found to vary nonlinearly with distance flown. The data reduction procedure developed, thus had to be applicable when nonlinear damping, transverse- and roll-angular rates are present.

With aerodynamic trim angles of up to 5° and frequency variations of 100 to 500% for bistable flights, the deviations between linear curve and data at low angles, due to aerodynamic nonlinearities, are virtually an order of magnitude larger than the trim due to asymmetry. The linear fit will therefore determine a large nontrim, roll-dependent vector. A concomitant of these circumstances is that when curve fits are determined at different roll rates p, and if the quality of a fit is evaluated on a basis of rms error, then the best tricyclic fit of the oscillation data will, in general, occur at a different p-value from that for the best fit of the swerve data. The first step in the data reduction procedure for local aerodynamic coefficients is then to determine an effective roll rate p_{EFF} from a series of curve fits at several possible roll rates input to the program, after which the primary fit, Eq. (4), is obtained. After transformation to the aeroballistic system, the oscillation data are smoothed by Eq. (5) and aeroballistic coordinates β and α generated at interval Δx. Subsequently, the flight distance X_c and the roll rate interpolated from measured roll data $p_3 = p(X_c)$ is determined at each angular peak. Finally, the local C_{m_α} is computed at each peak.

To determine C_{L_α}, $C_{L_q} + C_{L_{\dot\alpha}}$ and $C_{m_q} + C_{m_{\dot\alpha}}$, p_{EFF} is of course not applicable and the roll rate interpolated from measured data $p_1 = p(X_m)$ is used.

Free-Flight Test Details

The experimental program, comprising tests of stable and bistable configurations of the high-maneuverability model, was conducted in the CSIR Blowdown Tunnel at Mach 0.7.

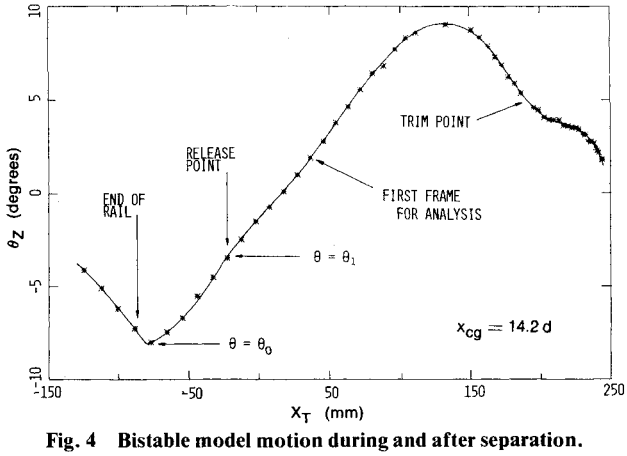

Fig. 4 Bistable model motion during and after separation.

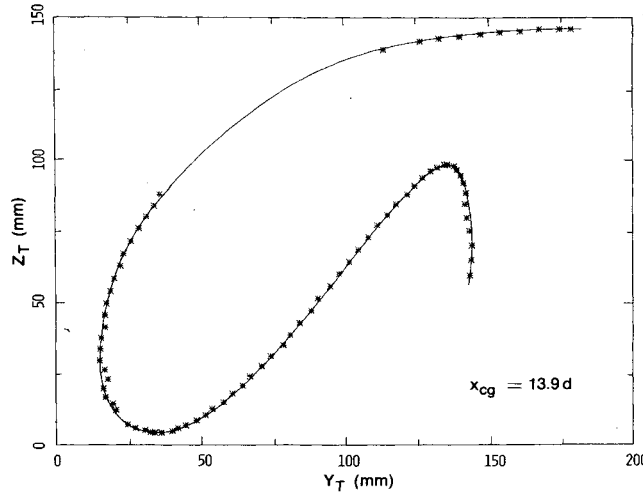

Fig. 5 Bistable model motion in the transverse plane.

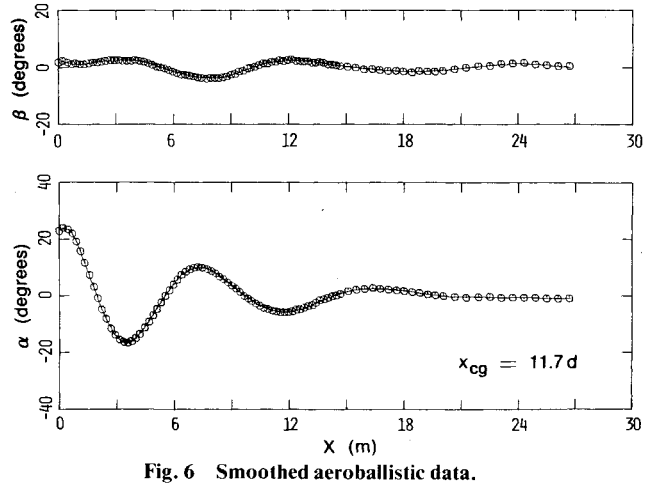

Fig. 6 Smoothed aeroballistic data.

Specifically, the approach was to a) document extensively dynamic and static data at two prime center-of-mass (cg) locations, $x_{\mathrm{cg}} = 11.7\,d$ and $x_{\mathrm{cg}} = 13.9\,d$; b) obtain data over the range of cg positions; and c) obtain additional data at higher frequencies for the stable-reference cg position. Of a total of 29 flights recorded, 25 were suitable for analysis (two models were too close to resonance and a further two were damaged). Results of the reduction of 14 flights are presented here.

In the case of models launched by means of the pitch-jet system, the first frame for analysis is chosen at a point one tail-span upstream of the release point and an equivalent distance beneath this point. In one flight, however, a number of downstream frames were analyzed in addition, with a view to studying the launch-head/model separation. The $\theta_z - X_T$ motion of this near-planar flight is depicted in Fig. 4. The curve comprises an initial pitch-down motion as it leaves the rail, followed by an acceleration section, and motion through a peak, after the model is free of interference.

Motion Documentation

Examples of the motion documentation are shown in Figs. 5 to 10. Figure 5 depicts the motion of a bistable model with mass center at $x_{\mathrm{cg}} = 13.9\,d$ in the tunnel reference system. With a displacement of 210 mm in the $Z_T - Y_T$ plane, compared with the depth of 220 mm of the observation rhombus, it will be appreciated that the magnitude of the swerving motion is close to the maximum that can be accommodated. In all flights the trajectories exhibit a characteristic, twisted figure-8 loop which allows the model to remain in sight while it traverses the viewing area in both upstream and downstream directions.

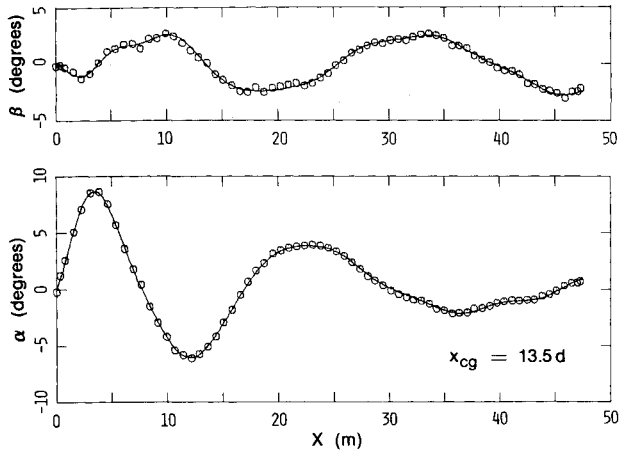

Fig. 7 Bistable model flight.

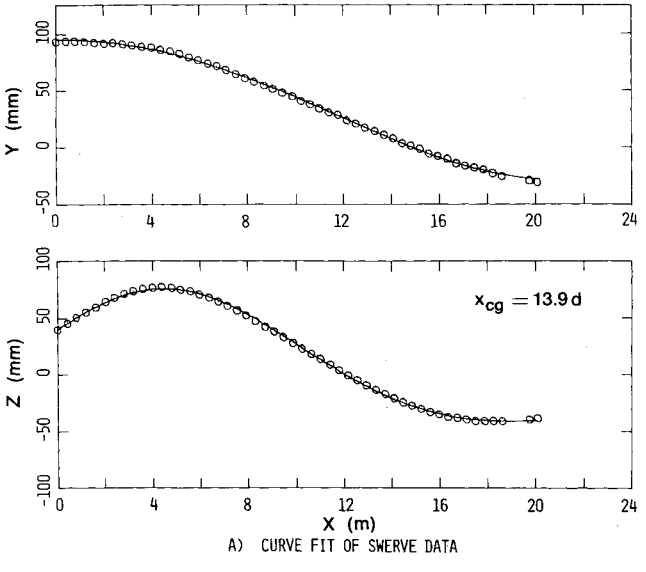

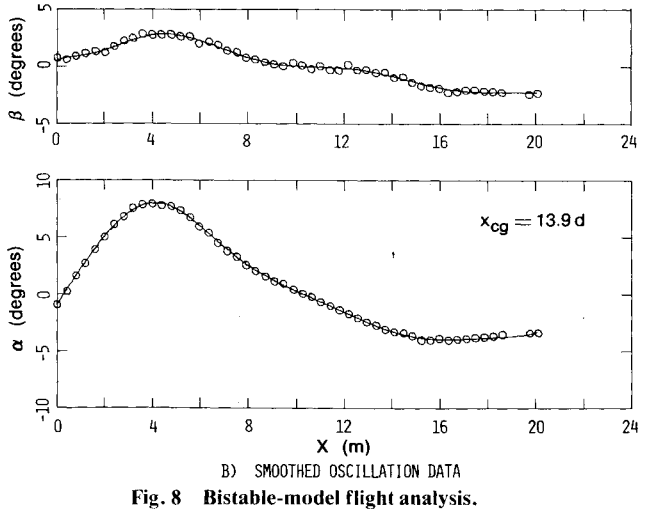

Fig. 8 Bistable-model flight analysis.

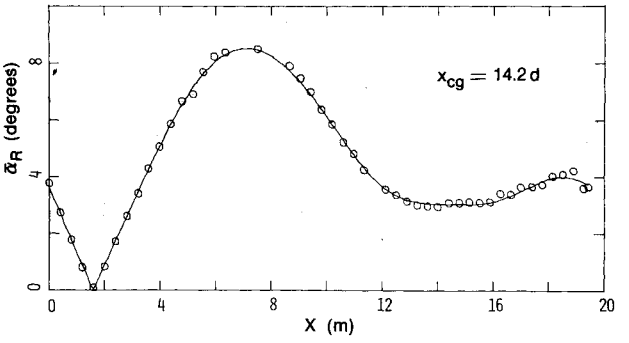

Fig. 9 Nonoscillating bistable model.

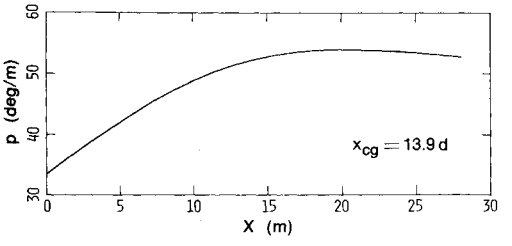

Fig. 10 Roll rate as a function of distance flown.

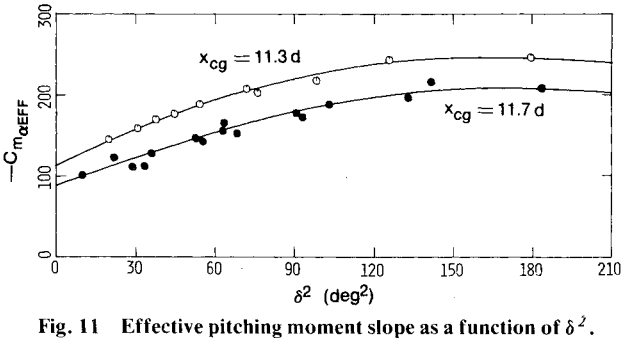

Fig. 11 Effective pitching moment slope as a function of δ^2.

The result of applying the smoothing procedure is shown in Fig. 6 for the case of a low-I_y stable flight. This flight contains a redundancy of data points, measured to determine the optimum number of points required. In the present tests, where the rms deviations were typically 0.13°, about 20 points per cycle were sufficient. With improvements to the camera optics made subsequent to these tests, deviations are around 0.05°, and perhaps 10 points per cycle would suffice.

A less stable flight, shown in Fig. 7, is close to the limit-cg position for bistable motion. Curve fits of the lateral displacement data and the smoothed aeroballistic angles are depicted in Fig. 8 for a bistable model (part of the trim motion is omitted).

Figure 8b exhibits the same type of "kink" present in the simulated flight (Fig. 2). The most unstable configuration tested, shown in Fig. 9, presents an example of a motion which fails to pass through the unstable condition and settles down to a trim angle of ~5°. Figures 8 and 9 therefore respectively exemplify limit cases for half-cycle oscillatory and nonoscillatory motion at approximately the same initial conditions.

Control of Roll Rates

Both stable and bistable models had a tendency to approach resonance. The roll behavior was due to induced rolling moments and small asymmetries rather than disturbance during launching. Unless roll direction can be predicted, there is no way that the motion of a bistable model after the initial oscillation peak can be "controlled" by trajectory design.

The procedure followed in the case of bistable models was to introduce a small difference in the lateral position of left- and right-hand nozzles relative to the tail surfaces. An adequate amount of prespin ensured that the roll rate would be above resonance and the motion be inhibited to follow a particular direction. An example of the roll-rate variation for a bistable model is depicted in Fig. 10.

Due to the higher oscillation frequencies, stable-model roll rates had to be limited to below resonance. As these models appeared to favor a particular roll direction, two thin wedges were glued to tail surfaces to produce a roll torque in the op-

posite direction. The resulting roll rates were at less than half the resonance rate.

Results

Since it is much more convenient to determine the dynamic stability coefficient $C_{mq}+C_{m\dot{\alpha}}$ from stable-model tests, the approach used was to obtain detailed data at the stable-reference configuration, $x_{cg}=11.7\ d$, and subsequently to evaluate the effect of oscillation frequency and center of mass to determine the applicability of these data to bistable flights. Lift-slope coefficients, C_{L_α}, and drag coefficients $C_{D\text{EFF}}$ were obtained both from stable and bistable flights.

Linear Stability Analysis

Figure 11 contains the $C_{m_{\alpha\text{EFF}}}$ data as a function of the mean-square resultant angle-of-attack δ^2, extracted from three flights of the reference configuration $x_{cg}=11.7\ d$ and one flight of the configuration $x_{cg}=11.3\ d$. The concept of an effective pitching-moment slope is not too meaningful here; however, the $C_{m_{\alpha\text{EFF}}}$ data serve to provide confidence in the local C_{m_α} data which are altogether more sensitive to the conditions of analysis.

Damping-in-pitch coefficients given in Fig. 12, were determined at two mean oscillation frequencies for the stable-reference configuration. The data appear to suggest a slight increase in dynamic stability with frequency. However, more flights would have to be analyzed to isolate this effect. Also, more careful choice of intervals could improve the correlation. The dynamic lift coefficient data (Fig. 13) showed a larger scatter which may be due, in part, to the fact that not all these data were obtained at optimum roll rates.

Local Aerodynamic Analysis

Local pitching-moment slope data for the stable and bistable reference configurations are presented in Fig. 14 as a function of $\bar{\alpha}^2$ where, for the moment, $\bar{\alpha}$ is defined as the mean local angle of attack $\bar{\alpha}_m=(\alpha_{\max}+\alpha_{\min})/2$. The data show strong nonlinear variations, with a destabilizing trend at higher angles of attack, which is less apparent in the effective static stability variations (Fig. 11).

The C_{m_α} data scatter is considerably larger than that for $C_{m_{\alpha\text{EFF}}}$, as could be expected when it is recognized how sensitive the local data are to local waveform variations such as could be caused by possible flow deviations in the test section. A more significant cause is thought to be the manifestation of nonaxisymmetric (i.e. cruciform) aerodynamics. It may be expedient to correlate C_{m_α} with the angle γ defining the roll orientation with respect to the plane of the complex angle of attack, as well as with $\bar{\alpha}$, for each local analysis interval.

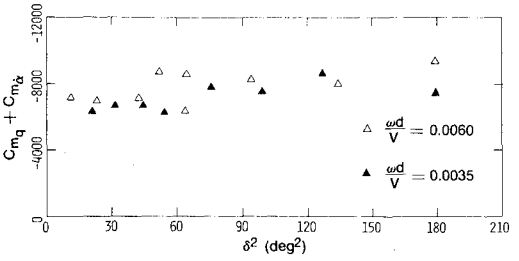

Fig. 12 Pitch-damping coefficient vs δ^2.

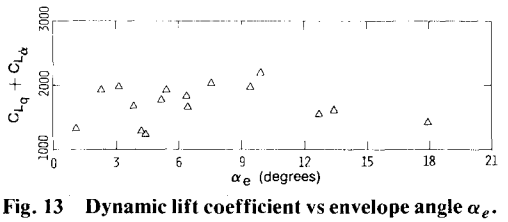

Fig. 13 Dynamic lift coefficient vs envelope angle α_e.

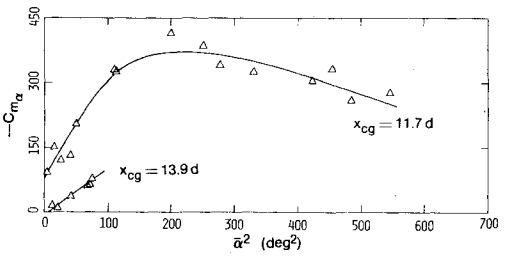

Fig. 14 Local pitching-moment slope as a function of $\bar{\alpha}^2$.

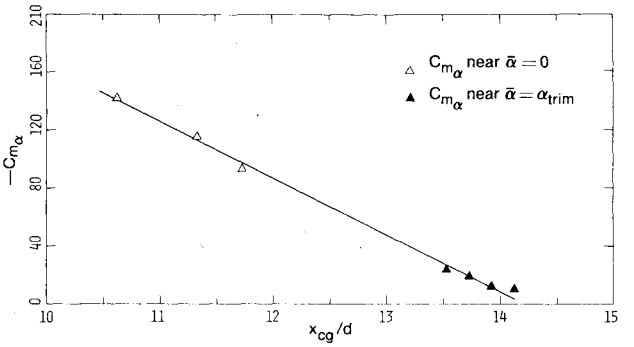

Fig. 15 Pitching-moment slope as a function of center-of-mass location.

Effect of Center of Mass

Figure 15 depicts the variation of static stability at low angles of attack with cg location aft of nose. In the case of the stable models, the values plotted were $C_{m_{\alpha 0}}$, obtained by extrapolating $C_{m_{\alpha\text{EFF}}}$ to $\delta^2=0$, while in the case of bistable models the values were C_{m_α} determined near α_{trim}. A similar comparison made for the dynamic stability coefficient $C_{mq}+C_{m\dot{\alpha}}$ indicated a slight trend of increasing dynamic stability with forward cg positions. However, this cannot be confirmed until more bistable model flights have been analyzed.

Evaluation of Results

Results of the test program presented in this paper have revealed interesting flight-dynamic phenomena. Most of the less-stable configurations exhibited transitions from planar to limit-circle motion, while cases of roll lock-in were observed. The validity of the test results was investigated by means of: a) a six-degree-of-freedom (6DOF) computer simulation generated using the data presented and initial conditions obtained for a particular flight; and b) a data comparison between free-flight and sting test results.

6DOF Simulation

The flight depicted in Fig. 8 was selected for the comparison. The simulation was based on free-flight drag and lift coefficients C_D and C_L, obtained from quadratic curve fits to $C_{D\text{EFF}}$ and C_{L_α} data, and free-flight pitching moment coefficients C_m and pitch damping $C_{mq}+C_{m\dot{\alpha}}$. Since the C_{m_α} were local values, a direct integration was possible. The curve at $x_{cg}=13.9\ d$ in Fig. 14 was first used to obtain a cubic pitching moment, $C_m=C\alpha+K\alpha^2$. When the simulated flight indicated that the $x_{cg}=13.9\ d$ free-flight data were too low, a bicubic pitching moment corresponding to the $x_{cg}=11.7\ d$ data was derived for the angle-of-attack range up to 10° and transformed to the $x_{cg}=13.9\ d$ reference. The resulting simulated flight shown in Fig. 16 compared well with the observed motion.

Returning to the data at $x_{cg}=13.9\ d$ in Fig. 14, possible causes of the disagreement here were considered: Bistable flight segments for local curve fits had relatively large ex-

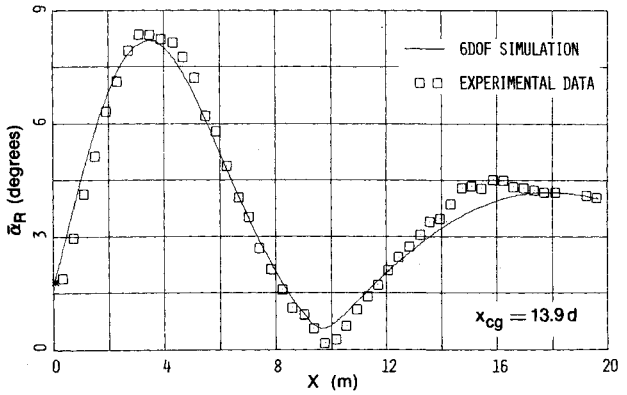

Fig. 16 Comparison of observed and simulated flights.

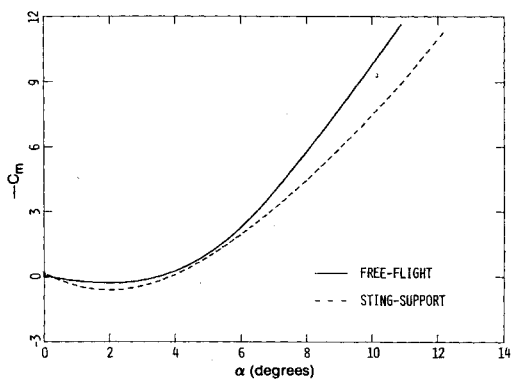

Fig. 17 Pitching-moment correlation.

cursions E [Eq. (6)]. An examination of the curve-fitting process suggested that it could be more correct to correlate C_{m_α} with $\bar{\alpha}^2 = \alpha^2_{\min}$ than with $\bar{\alpha}^2 = \bar{\alpha}^2_m$ or with $\bar{\alpha}^2 = \delta^2$. When this was done, the slope of the C_{m_α} curve increased and the correlation improved in Fig. 14. The new cubic pitching moment C_m obtained at $x_{cg} = 13.9\ d$ was in agreement with the C_m referred to $x_{cg} = 11.7\ d$.

Data Comparison

A direct comparison of free-flight and sting data determined in the Blowdown Wind Tunnel could be made. Normal force coefficients C_N derived from the C_D and C_L data compared favourably with C_N data measured on a sting. The free-flight values were consistently 8% lower than their static-test counterparts.

Figure 17 illustrates the correlation of pitching moment data from free-flight and sting-support tests for the low-angle-of-attack range corresponding to α_{max} for the simulated flight. Lower static stability is predicted by the sting data, particularly at higher angles of attack. In an effort to determine which curve is more representative of the real motion, the free-flight static coefficients C_N and C_m used in the simulation of Fig. 16 were replaced by sting-test coefficients. Comparison of this simulation with the observed data indicated a less satisfactory match, even after the initial conditions were adjusted.

It would thus appear that the free-flight static coefficients are more reliable than the corresponding sting test data at angles of attack. Since the free-flight C_N data are slightly lower and C_m higher than the sting test data, a calibration error in the sting test would appear to be unlikely and a significant effect due to sting interference is apparent.

Conclusions

Wind-tunnel free-flight testing techniques introduced in this paper have made possible repeatable flights of destabilized configurations under convenient laboratory conditions. The problem of analyzing these flights, which are essentially nonoscillatory at moderate angles of attack, is solved by the use of a local curve-fitting technique. Comprehensive wind-tunnel free-flight data for a canard-missile configuration, and in particular, local pitching-moment slopes extracted from angular peaks of both oscillatory and nonoscillatory free-flight motions, are presented here for the first time.

A 6DOF simulation, generated from the free-flight data presented, showed satisfactory agreement with the observed bistable model motion, while a correlation of free-flight and sting-test data indicated lower static stability in the latter case. This would suggest that the free-flight data were accurately determined and that sting interference was significant. An attempt to determine frequency effects on dynamic stability has, as yet, not been conclusive. Further work, which includes analysis of the remaining flights to obtain more well-correlated damping data and a correlation of local static stability data with the roll-orientation angle, may shed light on some of the questions posed by the results presented here.

The main conclusion which may be drawn here is that representative free-flight static and dynamic coefficients for high-maneuverability missiles and airplane-like configurations, which exhibit large lateral flight-path displacements, can be obtained in a wind tunnel.

References

[1] De Rose, C. and Boissevain, A. G., "An Exploratory Investigation in a Ballistic Range of the Stability Derivatives of a Simple Airplane Configuration at Low Supersonic Speeds," NASA TN D-139, Dec. 1959.

[2] Jaffe, P., "Nonplanar Tests Using the Wind-Tunnel Free-Flight Technique," *Journal of Spacecraft and Rockets*, Vol. 10, July 1973, pp. 435-442.

[3] Holmes, J. E. and Woehr, F. A., "Wind Tunnel Free-Flight Testing of Configurations with High-Fineness Ratio Bodies," AIAA Paper 71-278, Albuquerque, New Mex., 1971.

[4] Beyers, M. E., "Free-Flight Testing of High-Maneuverability Missile Configurations," CSIR Report ME 1453, Pretoria, South Africa, March 1976.

[5] Beyers, M. E., "Technique for Smoothing Free-Flight Oscillation Data," *Journal of Spacecraft and Rockets*, Vol. 12, May 1975, pp. 318-319.

[6] Beyers, M. E., "A New Technique for the Analysis of Non-Linear Free-Flight Motion," AIAA Paper 74-614, Bethesda, Md., 1974; also *Journal of Spacecraft and Rockets*, Vol. 12, May 1975, pp. 318-319.

[7] Dayman, B., Jr., "Free-Flight Testing in High-Speed Wind Tunnels," AGARDograph 113, May, 1966.

[8] Beyers, M. E., "Free-Flight Testing in the CSIR Blowdown Tunnel," CSIR Report ME 1191, Pretoria, South Africa, March 1973.

[9] Chapman, G. T. and Kirk, D. B., "A Method for Extracting Aerodynamic Coefficients from Free-Flight Data," *AIAA Journal*, Vol. 8, April 1970, pp. 753-758.

[10] Nicolaides, J. D., "On the Free-Flight Motion of Missiles having Slight Configurational Asymmetries," Ballistics Research Labs., Aberdeen Proving Ground, Md., BRL Report 858, June 1953.